Available online at www.sciencedirect.com
SCIENCE DIRECT
Journal of Power Sources 152 (2005) 60–66
JOURNAL OF POWER SOURCES
www.elsevier.com/locate/jpowsour

Simulation of the current density distribution for a PEMFC by using measured electrochemical and physical properties of the membrane☆

Takuto Araki*, Hironori Koori, Takuya Taniuchi, Kazuo Onda

Department of Electrical and Electronic Engineering, Toyohashi University of Technology 1-1 Hibarigaoka, Tenpaku, Toyohashi, Aichi 441-8580, Japan

Received 30 November 2004; accepted 27 December 2004
Available online 1 August 2005

Abstract

In order to grasp properly PEFC power generation performances, it is necessary to know aspects of water management such as transmissivity and electro-osmotic coefficient of water vapor through the membrane, and factors for power loss such as active and resistive overpotentials. In this study we have measured these factors to analyze our experimental results of PEFC power generation tests by our two-dimensional simulation code. It considers simultaneously the mass, charge and energy conservation equations, and the equivalent electric-circuit for PEFC to give numerical distributions of hydrogen/oxygen concentrations, current density, and gas/cell-component temperatures. The numerical distributions of current density under various operating conditions agreed well with the measured distributions by segmented electrodes, which had grooves for hydrogen/oxygen supply and were molded in our test cell being electrically insulated. Hydrogen/oxygen concentration changes measured by gas chromatography along the gas supply grooves gave also the experimental current distributions, which coincided almost with those by the segmented electrodes. Factors to correct the small difference between the measured and the calculated are also discussed from the stand point of the physical meaning of the calculated results considering factors which are not taken into account in our code.

Keywords: Polymer electrolyte fuel cell; Current density distribution; Membrane properties measurement; Numerical model of PEFC

1. Introduction

Establishing the precise numerical model for the proton exchange membrane fuel cell (PEMFC) provides a useful method to estimate and improve PEMFC performance. The first objective of the present investigation was to build a numerical model, which can describe the PEMFC performance such as a *V–i* characteristics and current distributions inside the cell. For properly building the PEMFC model, it is necessary to know the water management factors such as transmissivity and electro-osmotic coefficient of water vapor through the membrane-electrode assembly (MEA), and power loss factors such as activation and resistive overpotentials, since these factors have significant impact on the performance of the PEMFC. Nevertheless, the effects of these factors on the PEMFC have not been defined sufficiently. Then, obtaining the basic information for PEMFC is a second objective of this study. A comparison of measured and calculated current distributions is finally conducted to verify the reliability of our numerical model. This comparison between power generating experiments and numerical simulations on the same cell configuration has rarely been reported before. The numerical distributions of current density under various operating conditions agreed well with the measured distributions by segmented electrodes, which had grooves for the hydrogen/oxygen supply and were molded in our test cell being electrically insulated. Hydrogen/oxygen concentration changes measured by gas chromatography along the gas supply grooves also gave the experimental current

☆ This paper was presented at the 2004 Fuel Cell Seminar, San Antonio, TX, USA.

* Corresponding author. Tel.: +81 532 44 6728; fax: +81 532 44 6728.
E-mail address: araki@eee.tut.ac.jp (T. Araki).

0378-7753/$ – see front matter © 2005 Elsevier B.V. All rights reserved.
doi:10.1016/j.jpowsour.2004.12.058

Nomenclature

A	membrane active area (cm^2)
a	relative humidity
C	gas concentration ($g\,cm^{-3}$)
D_i	diffusion coefficient of species i ($m^2\,s^{-1}$)
d_l	thickness of layer l (cm)
E°	standard electromotive force (V)
F	Faraday constant ($C\,mol^{-1}$)
f	effective porosity of diffusion electrode
H_{m-T}	enthalpy of species m at T (K) ($J\,mol^{-1}$)
$h(v)$	mass transfer coefficient at flow velocity v ($cm\,s^{-1}$)
i_m	averaged current density ($A\,cm^{-2}$)
i	local current density ($A\,cm^{-2}$)
k	heat conductivity ($W\,cm^{-1}\,K^{-1}$)
M_x, M'_x	vapor flow rate ($g\,s^{-1}$)
M_e	vapor flow rate of generated water ($g\,s^{-1}$)
M_{OSM}	vapor flow rate of electro-osmosis ($g\,s^{-1}$)
N	molar velocity of x direction ($mol\,cm^{-2}\,s^{-1}$)
n_d	electro-osmotic coefficient
P_i	partial pressure of gas species i (atm)
R	gas constant ($J\,mol^{-1}\,K^{-1}$)
R_l	gas diffusive resistance of a layer l
T_{mem}	temperature of MEA (K)
Tr	transmissivity of MEA ($cm^2\,s^{-1}$)
V_{cell}	cell voltage (V)
V_{Nernst}	Nernst potential (V)
v	supplied gas velocity ($m\,s^{-1}$)
w_{cell}	cell width (channel width + rib width) (cm)

Subscripts

ρ	membrane resistance ($\Omega\,cm^2$)
ρ	membrane resistivity (Ω cm)
η_{act}	activation overpotential (V)
η_{ohm}	resistive overpotential (V)

Subscripts

H_2, O_2, H_2O	hydrogen, oxygen and water, respectively
a, c	anode and cathode
liq, vap	liquid and vapor
mem	membrane
MEA	MEA
DIF	diffusion electrode

distributions, which coincided almost with those by the segmented electrodes. Factors to correct the small difference between the measured and the calculated are also discussed from the standpoint of the physical meaning of the calculated results considering factors, which are not taken into account in our code.

2. Measurements of membrane properties and overpotentials

2.1. Overview of experimental apparatus

An overview of the experimental apparatus is illustrated in Fig. 1 and is basically the same as in our previous paper [1]. Fuel (hydrogen or modified reformed fuel) and oxidant (oxygen or air) from gas cylinders were regulated by mass flow controllers, and led to the fuel cell (FC). The humidifiers placed before the FC, control the dew-point temperatures of air and fuel. An Electronic resistive load (PLZ-152WA, Kikusui Elec. Co.) was connected to the FC instead of actual loading, and measured the current and voltage of the FC. The MEA (Gore Select, Japan Gore-Tex Inc.) of 20 μm thickness is set between the two electrodes and carbon cloths are inserted between the MEA and separators as diffusion electrodes. One side of which consisted of segmented electrodes with grooves for air or fuel supply and the segmented electrodes are molded in an electrically insulating plate for measuring current density distributions. Additionally, several holes are drilled in the grooves to measure concentration changes of hydrogen and oxygen to get another current density distribution. More information on the experimental conditions will be given in each section.

2.2. Water-vapor diffusivity through diffusion electrodes, transmissivity and electro-osmotic coefficient through the MEA

To obtain the diffusive properties, the cell outlet average humidities at both anode and cathode were measured by supplying different humidities to both FC inlets. The amounts of vapor transport through each layer M_x can be written as follows, while considering the mass transfer coefficient $h(v)$ between gas diffusion electrode (GDL) and channel flow.

$$M_x = h_a(v)(C_a - C_{a,\,DIF})A \quad (1)$$

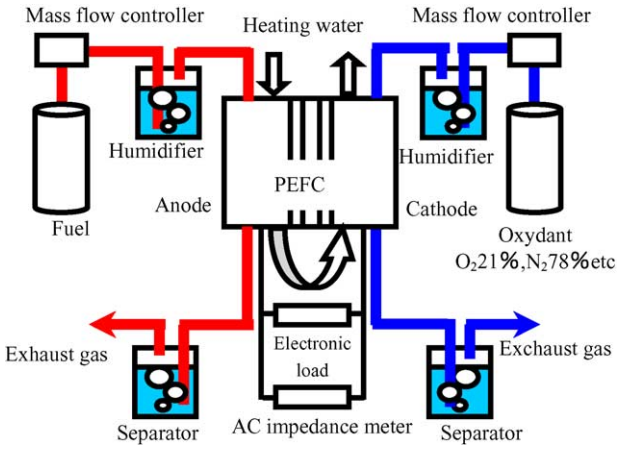

Fig. 1. Experimental apparatus.

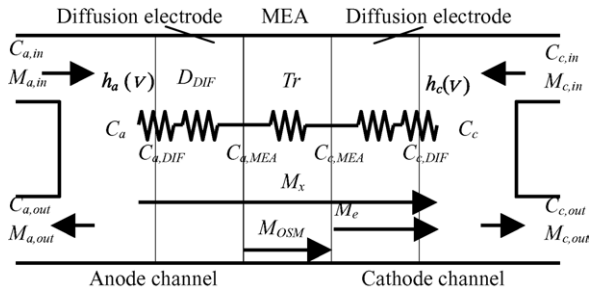

Fig. 2. Transport model of water-vapor in PEFC.

$$M_x = \frac{D_{\mathrm{DIF}}(C_{\mathrm{a,\,DIF}} - C_{\mathrm{a,\,MEA}})A}{d_{\mathrm{DIF}}} \tag{2}$$

$$M_x = \frac{\mathrm{Tr}(C_{\mathrm{a,\,MEA}} - C_{\mathrm{c,\,MEA}})A}{d_{\mathrm{MEA}}} \tag{3}$$

$$M_x = \frac{D_{\mathrm{DIF}}(C_{\mathrm{c,\,MEA}} - C_{\mathrm{c,\,DIF}})A}{d_{\mathrm{DIF}}} \tag{4}$$

$$M_x = h_{\mathrm{c}}(v)(C_{\mathrm{c,\,DIF}} - C_{\mathrm{c}})A \tag{5}$$

$$\frac{C_{\mathrm{a}} - C_{\mathrm{c}}}{M_x} = \frac{1}{h_{\mathrm{a}}(v)\cdot A} + \frac{1}{h_{\mathrm{c}}(v)A} + 2\frac{d_{\mathrm{DIF}}}{D_{\mathrm{DIF}}A} + \frac{d_{\mathrm{MEA}}}{\mathrm{Tr}\,A} = 2R_{\mathrm{l}}(v) + 2R_{\mathrm{DIF}} + R_{\mathrm{MEA}} \tag{6}$$

Here d_{l}, D_{DIF}, Tr and C_i denotes the thickness of layer l, diffusion coefficient of GDL, transmissivity through MEA and concentration of vapor at boundary of two layers. The pattern diagram of this water (vapor) transport model is depicted in Fig. 2. Considering the values of M_x of Eqs. (1)–(4) are equal in steady flow, Eq. (5) is derived. The $h(v)$ increased as gas velocity v increasing, and the diffusive resistance $R_h(v) = 1/h(v)\cdot A$ was relatively much smaller than R_{DIF} and R_{MEA}, so that the effect of the mass transfer can be ignored in our experimental conditions.

Measured water vapor diffusivity for diffusion electrode D_{DIF} at cell temperature $T_{\mathrm{mem}} = 50$ and 60 °C are plotted in Fig. 3. The diffusivity did not change against relative humidity. This result is consistent with a simple following equation:

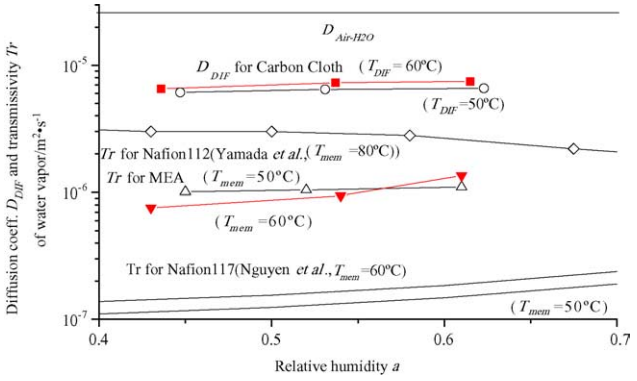

Fig. 3. Change of diffusion coefficient D_{DIF} and transmissivity Tr by temperature T_{mem} and relative humidity.

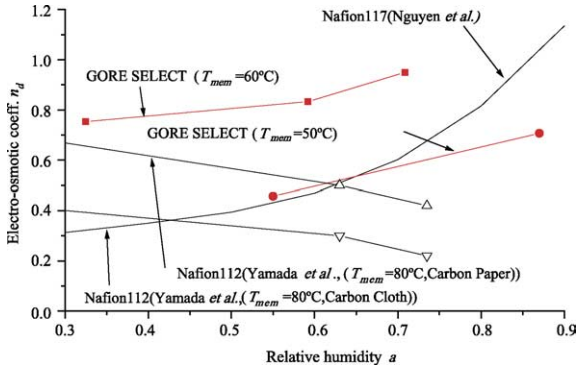

Fig. 4. Change of electro-osmotic coefficient by temperature and relative humidity.

$$D_{\mathrm{DIF}} = fD_{\mathrm{air\text{–}H_2O}} \tag{7}$$

where $D_{\mathrm{air\text{–}H_2O}}$ is water vapor diffusivity in air, and f the effective porosity of diffusion electrodes. In the case of out carbon cloth, f is calculated to be about 0.25.

Transmissivity through MEA Tr is also shown in Fig. 3. Our measured Tr was about 7 times higher than the ones by Nguyen and White [2] and lower than ones by Yamada and Morimoto [3]. However, the tendency of Tr, which rose as relative humidity increase, was consistent with those by Nguyen et al. So we approximate Tr as to 7 times greater than those of Nguyen et al.

The electro-osmotic coefficient n_d is obtained from the equations shown below and the measured D_{DIF} and Tr.

$$M'_x = h_{\mathrm{a}}(v)(C_{\mathrm{a}} - C_{\mathrm{a,\,DIF}})A \tag{8}$$

$$M'_x = \frac{D_{\mathrm{DIF}}(C_{\mathrm{a,DIF}} - C_{\mathrm{a,MEA}})A}{d_{\mathrm{DIF}}} \tag{9}$$

$$M'_x = \frac{\mathrm{Tr}(C_{\mathrm{a,MEA}} - C_{\mathrm{c,MEA}})A}{d_{\mathrm{MEA}} + M_{\mathrm{OSM}}} \tag{10}$$

$$M'_x = \frac{D_{\mathrm{DIF}}(C_{\mathrm{c,MEA}} - C_{\mathrm{c,DIF}})A}{d_{\mathrm{DIF}} - M_e} \tag{11}$$

$$M'_x = h_{\mathrm{c}}(v)(C_{\mathrm{c,DIF}} - C_{\mathrm{c}})A - M_e \tag{12}$$

M_e and M_{OSM} are water flow rate by generated water and electro-osmosis. Then the electro-osmotic coefficient n_d is expressed as:

$$n_d = \frac{M_{\mathrm{OSM}}}{18}\frac{F}{I}. \tag{13}$$

F is Faraday constant and I the current through the cell. Fig. 4 shows the n_d as a function of relative humidity. The electro-osmotic coefficient n_d became large when the humidity increases. n_d at MEA temperature of 50 °C agreed with that by Nguyen et al. n_d by Yamada who performed similar experiment with us was almost same as ours, especially in a case of using carbon cloth, however, the tendency of n_d against humidity was inverse.

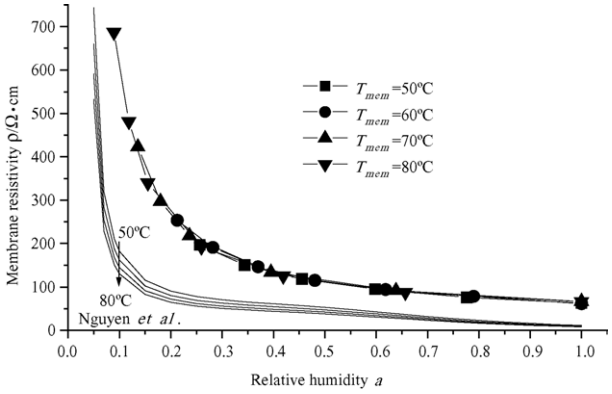

Fig. 5. Change of membrane resistance by temperature and relative humidity.

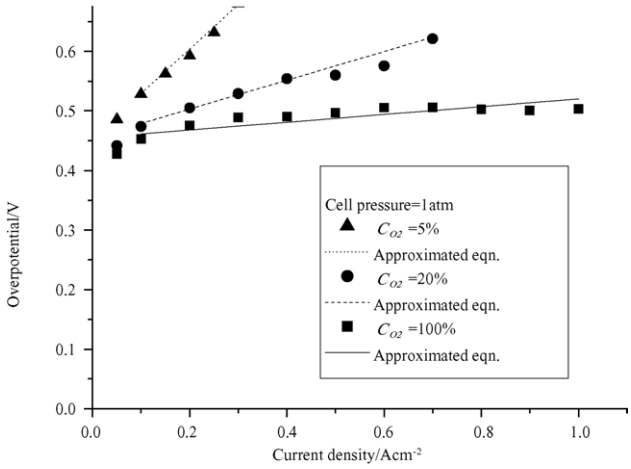

Fig. 6. Change of overpotential by oxygen concentration and current density.

2.3. Ionic resistivity and activation overpotential of the MEA

Resistive and active overpotentials are important factors in PEFC power generation performance. The ionic resistance was measured by AC impedance meter (SOLARTRON SI1280B), supplying air with the same humidity to both anode and cathode to avoid the movement of water through the MEA. The parameters for MEA resistance are the membrane temperature T_{mem} and the flow relative humidity a. The measured MEA resistivity is plotted against relative humidity a in Fig. 5. The resistivity did not depend on the membrane temperature, but depended only on the relative humidity a. Therefore, the following experimental ionic resistivity ρ, a function of only relative humidity a, was employed in the following numerical analysis.

$$\rho = 57.3 + 383 \exp\left(-\frac{a - 0.089}{0.049}\right) + 244 \exp\left(-\frac{a - 0.089}{0.268}\right) \quad (14)$$

For measuring activation overpotential η_{act}, the relatively high flow rates of 600 cc min^{-1} were provided to hold the low utilization rate of H_2 and O_2 in order to prevent variation of η_{act} along the flow by the distributed current density. η_{act} was derived by subtracting the cell voltage V_{cell} and the resistive overpotential ir from the Nernst potential V_{Nernst} as follows:

$$\eta_{\text{act}} = V_{\text{Nernst}} - V_{\text{cell}} - ir \quad (15)$$

Here, the spatially averaged partial pressures of active materials were used to determine V_{Nernst} considering water vapor pressures. The experimental conditions for η_{act} measurement were as follows; FC temperature: 60 °C, cathode O_2 partial pressure P_{O_2}: 0.05, 0.2, 1.0; anode H_2 partial pressure P_{H_2}: 1.0. Fig. 6 shows the change of activation overpotential by oxygen concentration and current density. The activation overpotential increased almost linearly except for the region of very low current density where is not so important for practical applications. Therefore, we employed the following empirical formula in the following numerical analysis.

$$\eta_{\text{act}} = \frac{0.065}{P_{O_2}^{0.81}} i + 0.455 \quad (16)$$

3. Measurement of current distributions

Current distributions were measured by two different methods to confirm the reliability of the measurements. The first method used the segmented electrodes cell to measure the current distribution by shunt resistances. Another method used gas chromatography to measure gas composition changes to be converted to the current distribution through the decreased flow rate of H_2 or O_2. N_2 mixture fuel and air were employed in this measurement to keep the constant flow rate of N_2 as a reference. H_2 gas mixed with 20% N_2 (not CO_2) was used as the fuel, because CO_2 is easy to be solved in water and not giving the correct reference. The cell configuration for current distribution measurement is illustrated in Fig. 7.

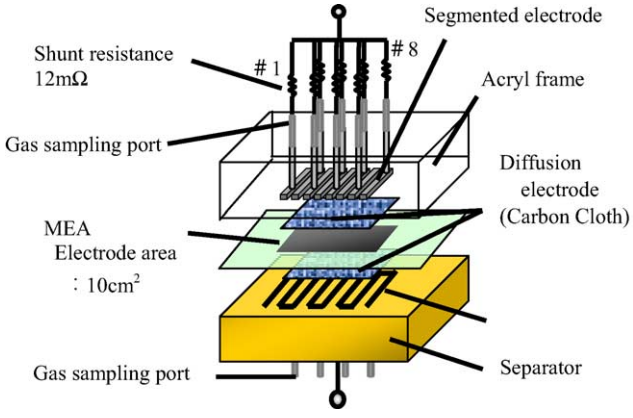

Fig. 7. Configuration of cell and segmented electrodes.

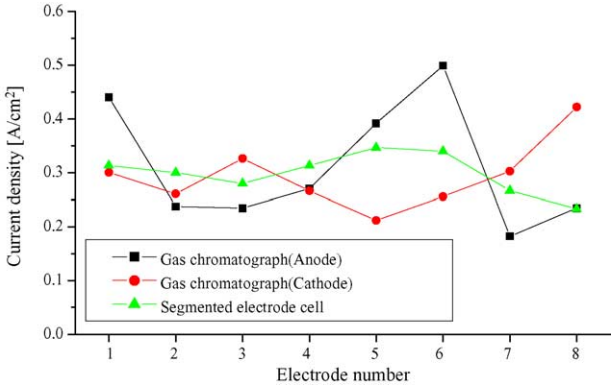

Fig. 8. Comparison of measured current distributions (i_m = 0.3 A cm^{-2}).

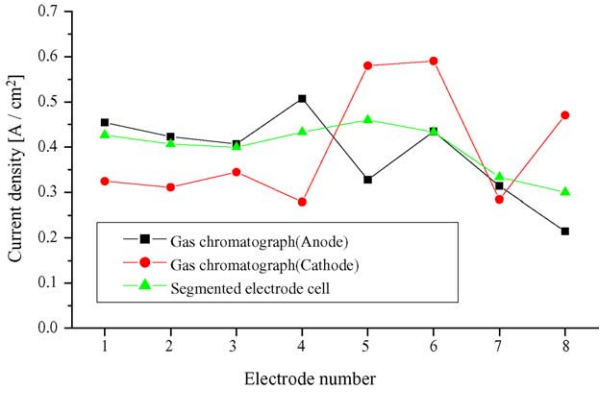

Fig. 9. Comparison of measured current distributions (i_m = 0.4 A cm^{-2}).

Figs. 8 and 9 shows the measured current density distributions for two average current densities i_m of 0.3 and 0.4 A cm^{-2}, respectively. The current density estimated by gas chromatography fluctuated to some extent, but was compatible with that measured by the segmented electrodes cell. Thus we could confirm the measurement reliability of current density distribution by two methods.

4. Numerical model of PEMFC

4.1. Numerical procedure

Our model basically consists of steady-state two-dimensional mass, charge and energy conservation equations with an equivalent electric circuit of the PEMFC. The following assumptions are adapted to derive the governing equations [4].

1. Fuel cell is a parallel flow type.
2. Gas flow along a channel is plug flow.
3. Owing to the constant-temperature water circulation through separators, the separator temperature is constant.
4. The volume of the condensed water is so small that the effect of condensed water at the cathode can be neglected.
5. The total gas pressure is constant, neglecting the pressure drop along the flow channel.

The mass conservation equations are as follows by using mole flow rate M_j of each chemical species j, and current density i through MEA. The subscripts a, c and k denote at anode, cathode and either anode or cathode, respectively. d the height (thickness) of channel (layer) and h the channel width.

$$\text{Hydrogen}: \quad \frac{\mathrm{d}M_{\mathrm{H_2}}}{\mathrm{d}x} = -\frac{hi}{2F} \tag{17}$$

$$\text{Oxygen}: \quad \frac{\mathrm{d}M_{\mathrm{O_2}}}{\mathrm{d}x} = -\frac{hi}{4F} \tag{18}$$

Water liquid :

$$\frac{\mathrm{d}M^{\mathrm{liquid}}_{\mathrm{water},k}}{\mathrm{d}x} = \left(\frac{hd_{\mathrm{channel}}}{R(T_k + 273.15)}\right) \times \left(\frac{M^{\mathrm{vapor}}_{\mathrm{water},k}}{M^{\mathrm{vapor}}_{\mathrm{water},k} + M_{\mathrm{H_2}}} P - P^{\mathrm{saturated}}_{\mathrm{water},k}\right) \tag{19}$$

Water vapor (anode) :

$$\frac{\mathrm{d}M^{\mathrm{vapor}}_{\mathrm{water,a}}}{\mathrm{d}x} = -\frac{\mathrm{d}M^{\mathrm{liquid}}_{\mathrm{water,a}}}{\mathrm{d}x} - \frac{\mathrm{d}M_{\mathrm{vapor}}}{\mathrm{d}x} \tag{20}$$

Water vapor (cathode) :

$$\frac{\mathrm{d}M^{\mathrm{vapor}}_{\mathrm{water,c}}}{\mathrm{d}x} = -\frac{\mathrm{d}M^{\mathrm{liquid}}_{\mathrm{water,c}}}{\mathrm{d}x} + \frac{\mathrm{d}M_{\mathrm{vapor}}}{\mathrm{d}x} + \frac{hi}{2F} \tag{21}$$

Here M_{vapor} is the water vapor mole flow rate from anode to cathode.

$$\frac{\mathrm{d}M_{\mathrm{vapor}}}{\mathrm{d}x} = \frac{R_{\mathrm{MEA}}\left(-\mathrm{Tr}(\mathrm{d}C_w/\mathrm{d}y) + n_d(i/F)\right) - R_{\mathrm{DIF,c}}(i/2F)}{R_{\mathrm{MEA}} + R_{\mathrm{DIF,a}} + R_{\mathrm{DIF,c}}}h \tag{22}$$

Five energy conservation different equations for five layers (two gas channels, two diffusion electrodes and one MEA) are derived, for instance, equations of MEA and diffusion electrode are shown below.

$$\text{MEA}: \quad t_{\mathrm{mem}}\frac{d}{\mathrm{d}y}\left(k_{\mathrm{mem}}\frac{\mathrm{d}T_{\mathrm{mem}}}{\mathrm{d}y}\right) = k_{\mathrm{diff,a\text{-}mem}}\frac{T_{\mathrm{mem}} - T_{\mathrm{DIF,a}}}{\Delta x_{\mathrm{DIF,a\text{-}mem}}} + k_{\mathrm{dif,c\text{-}mem}}\frac{T_{\mathrm{mem}} - T_{\mathrm{DIF,c}}}{\Delta x_{\mathrm{DIF,c\text{-}mem}}}$$

$$-\left(\sum_j N_{j,\mathrm{a}}H_{j-T_{\mathrm{dif,a}}} - \sum_j N_{j,\mathrm{c}}H_{j-T_{\mathrm{dif,c}}}\right) - N_{\mathrm{H_2}}\Delta H_{\mathrm{LHV}} + i(V_{\mathrm{Nernst}} - \eta_{\mathrm{ohm}} - \eta_{\mathrm{act}}) \tag{23}$$

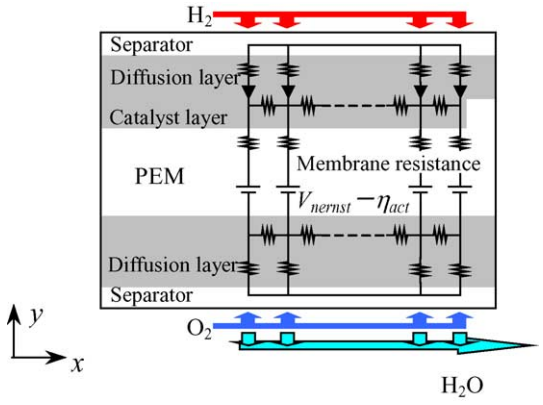

Fig. 10. Equivalent electric circuits for the PEFC.

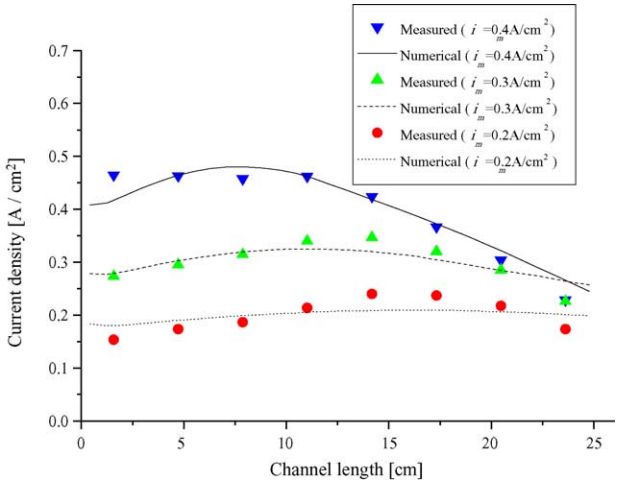

Fig. 11. Comparison between the measured and the numerical current distributions (air flow rate: 91 cc min^{-1}).

$$\text{DE}: \quad \sum_j (M_j c_{p,j}) \frac{\mathrm{d}T_k}{\mathrm{d}x} = (H^{\text{vapor}}_{\text{water},k} - H^{\text{liquid}}_{\text{water},k}) \frac{\mathrm{d}M^{\text{liquid}}_{\text{water},k}}{\mathrm{d}x} + U(T_s - T_k) \tag{24}$$

Here N_j and H_j represent the mole flux along y-direction and enthalpy of the j species, respectively. U is heat transfer coefficient. η_{ohm} is resistive overpotential by Eq. (25) as a function of the MEA resistivity ρ.

$$\eta_{\text{ohm}} = \left(\frac{1}{a_{\text{a}} - a_{\text{c}}} \int_{a_{\text{c}}}^{a_{\text{a}}} \rho \, \mathrm{d}a \right) t_{\text{mem}} i \tag{25}$$

The equivalent electric circuit for PEMFC is shown in Fig. 10. Due to the high electric conductivity of the separators, the cell voltage along channel can be kept constant. Control volume method and tri-diagonal matrix algorithm (TDMA) were used to solve simultaneously Eqs. (17)–(24) with an equivalent circuit [5].

4.2. Comparison of the current distributions with the measured

The current density distributions calculated by the numerical model are shown in Figs. 11–13. The conditions for the analysis and experiments are summarized in Table 1. The cathode flow was not humidified to observe the change of current density clearly. Distributions of current densities were increased from the inlet as the membrane water content

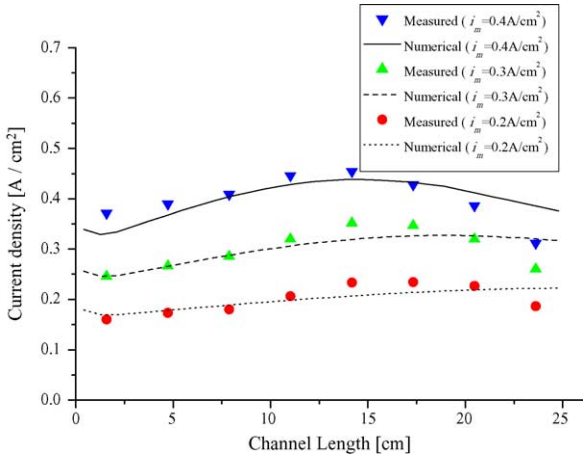

Fig. 12. Comparison between the measured and the numerical current distributions (air flow rate: 136 cc min^{-1}).

Table 1
Experimental conditions used in the numerical model

Figure number	11	12	13
Cell temperature (°C)		60	
Anode flow rate (cc min^{-1})		48	
Cathode flow rate (cc min^{-1})	91	136	182
Anode dew temperature (°C)		60	
Cathode dew temperature (°C)		Not humidified	
Fuel and oxygen utilization ratio (i_m =0.2 A cm^{-2})	0.4, 0.4	0.4, 0.26	0.4, 0.2
Fuel and oxygen utilization ratio (i_m = 0.3 A cm^{-2})	0.6, 0.6	0.6, 0.4	0.6, 0.3
Fuel and oxygen utilization ratio (i_m = 0.4 A cm^{-2})	0.6, 0.6	0.8, 0.53	0.8, 0.4

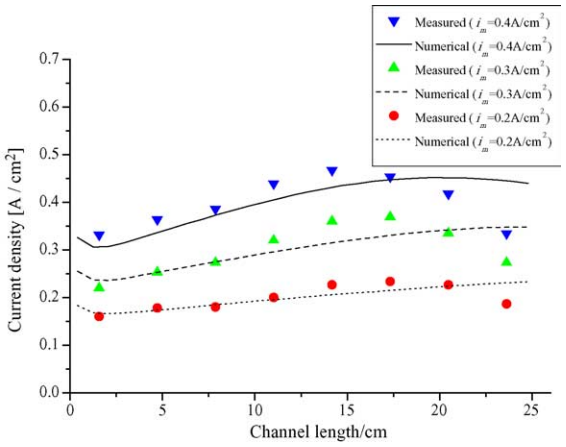

Fig. 13. Comparison between the measured and the numerical current distributions (air flow rate: 182 cc min^{-1}).

increases with generated water. Then, they decreased from around a middle of a flow channel, since the oxygen partial pressure decreased and the activation overpotential η_{act} increased along the channel. The position of the current peak was shifted downstream as the averaged current decreased, because lower i_m means lower water generation speed and lower oxygen consumption which leads to a smaller activation overpotential η_{act}.

The good agreement between the numerical and measured results indicates that our numerical model using the measured water management and power loss factors can provide a useful tool to estimate the PEMFC power generation performance. The measured results showed a higher current density at the inlet, and a lower current density at the outlet than the calculated results, especially for the higher oxygen utilization ratio of 80%. This discrepancy might be due to flooding by generated water at a downstream cathode, hindering the site for electrochemical reaction. Further studies are needed on the empirical formula for the activation overpotential, water management factors and diffusion overpotential through the diffusion electrode.

5. Conclusions

The water management factors such as transmissivity and electro-osmotic coefficient of water vapor through the membrane electrode assembly, and power loss factors such as activative and resistive overpotentials have been measured. These factors were used to analyze our experimental results for PEFC power generation tests by our two-dimensional simulation code. The code considers simultaneously the mass, charge and energy conservation equations with the equivalent electric-circuit for PEFC to give a numerical distribution of the hydrogen/oxygen concentrations, current density, and gas/cell-component temperatures along gas flow direction. The calculated distributions of current density under various operating conditions have agreed well with the measured distributions at the segmented-electrodes cell. Hydrogen/oxygen concentration changes measured by gas chromatography along the gas flow direction have also given the experimental current distributions, which coincide with that from the segmented-electrodes. Degradation factors for cell performance were also discussed from the numerical results using the simulation code. Also further improvements for our experiment and analysis have been discussed.

References

[1] T. Kyakuno, K. Hattori, K. Ito, K. Onda, Proceedings of the 2003 IEEJ Conference, 2003, 7-151 (in Japanese).
[2] T.V. Nguyen, R.E. White, Electrochem. J. Soc. 140 (8) (1993) 2178.
[3] H. Yamada, Y. Morimoto, in: Proceedings of the 70th Anniversary, Jpn. Electrochem. Soc. (2003) 316 (in Japanese).
[4] T. Aoki, N. Miyauchi, K. Ito, Y. Inui, K. Onda, Numerical analysis of polymer electrolyte fuel cell using empirical equations for overpotentials, Trans. IEE Jpn. 122-B (12) (2002) (in Japanese).
[5] S.V. Patankar, Numerical Heat Transfer and Fluid Flow, Hemisphere Publishing, 1985, pp. 24–56.